Supporting Information

Table of contents

Experimental section

1. Chemicals and reagents

All chemical reagents used in this study were purchased commercially and used without further purification. Nessler's reagent was obtained from Tianjin Jinke Fine Chemical Co., Ltd. Water-absorbent beads were purchased from Prudential (Zhongshan) New Materials Co., Ltd. Ascorbic acid, Potassium sodium tartrate, Potassium antimony tartrate, NaCl, KCl, LiCl, BaCl, $CaCl_2$, $MgCl_2$, CH_3COONa, NaI, Na_2CO_3, $NaNO_3$, $NiSO_4·6H_2O$, $CuSO_4$, $ZnSO_4$ $MnSO_4·4H_2O$, $CoSO_4·7H_2O$, NaH_2PO_4, NH_4Cl, $(NH_4)_6Mo_7O_2·4H_2O$, $FeSO_4·7H_2O$, $NH_2OH·HCl$ and 1,10-phenanthroline were obtained from Shanghai Macklin Biochemical Co., Ltd.

2. Instruments and devices

The precision pH meter (PHS-3C) was purchased from Shanghai Precision Science Instrument Co., Ltd. The analytical balance (BSA124S) was purchased from Sciencetech Instruments (Beijing) Co., Ltd. The smart camera (SHL-500) was purchased from Shenzhen Shunhuali Electronics Co., Ltd. The UV-Vis spectrophotometer (TU1901) was purchased from Beijing Plexin General Instrument Co., Ltd.

3. Preparation of colorimetric PAAHM sensor

3.1. Preparation of NH_4^+ colorimetric PAAHM sensor

Nessler's reagent was first diluted to one-fifth of its original concentration and subsequently mixed with a 0.272 mol/L potassium sodium tartrate solution at a volume ratio of 2:1. A total of 100 hydrogel microspheres were immersed in 10 mL of the mixed solution for 10 min. After loading, the microspheres were retrieved and allowed to stabilize prior to analytical use.

3.2. Preparation of PO_4^{3-} colorimetric PAAHM sensor

A molybdate solution (0.105 mol/L), an ascorbic acid solution (0.568 mol/L), and a potassium antimony tartrate solution (0.0108 mol/L) were mixed at a volume ratio of

3:2:2. The pH of the mixed solution was adjusted to 3.0. Subsequently, 100 hydrogel microspheres were immersed in 10 mL of the prepared solution for 2 min. The loaded microspheres were then retrieved and stabilized before further use.

3.2. Preparation of Fe^{2+} colorimetric PAAHM sensor

One hundred hydrogel microspheres were immersed in 5 mL of 1,10-phenanthroline solution (0.00833 mol/L) for 5 min. The microspheres were subsequently retrieved and allowed to stabilize prior to analytical application.

4. Actual water sample collection source

Actual water samples were collected from Guangzhou City, Guangdong Province, including samples from the Guangzhou Airport Sewage Treatment Plant Inlet, Hai Tao Phase III Inlet, Qian Feng Phase I & II Inlet, Li Jiao Phase I & II Inlet, and Lie De Phase I & II Inlet. For more details, please refer to Table S1. Water samples were collected, preserved and handled in accordance with the established protocols for sampling water quality (ISO 5667-3:2024)[1].

5. Pretreatment of Real Water Samples for UV-Vis Determination of NH_4^+

Prior to NH_4^+ determination by UV-Vis spectrophotometry, real water samples were pretreated by distillation to eliminate potential interferences (HJ 535-2009)[2]. Briefly, 50 mL 0.323 mol L^{-1} boric acid solution was transferred into a receiving flask. 250 mL water sample was placed into a distillation flask, followed by the addition of several drops of bromothymol blue indicator. The sample pH was adjusted to 6.0-7.4 using sodium hydroxide or hydrochloric acid solution as required. Subsequently, 0.25 g of light magnesium oxide and several glass beads were added, and the distillation apparatus, including the ammonia gas trap and condenser, was immediately assembled. The mixture was then heated for distillation, maintaining a distillate flow rate of approximately 10 mL min^{-1}.

6. Condition optimization of colorimetric PAAHM sensor

6.1. Condition optimization of PO_4^{3-} colorimetric PAAHM sensor

Optimization of Ascorbic acid Concentration: to optimize the concentration of ascorbic acid, solutions containing 0.105 mol/L $(NH_4)_6Mo_7O_{24}$, 0.0108 mol/L potassium antimony tartrate, and PO_4^{3-} at concentrations ranging from 1×10^{-5} to 1×10^{-2} mol/L were prepared. The ascorbic acid concentration was varied from 0.0568 mol /L to 0.568 mol /L. After the colorimetric reaction, images of the samples were acquired, and the corresponding RGB values were extracted. The experimental results are summarized in Figure S1.

Optimization of Potassium antimony tartrate Concentration: for optimization of the potassium antimony tartrate concentration, solutions containing 0.105 mol/L $(NH_4)_6Mo_7O_{24}$, 0.568 mol/L ascorbic acid, and PO_4^{3-} (1×10^{-5}-1×10^{-2} mol/L) were prepared. The concentration of potassium antimony tartrate was varied from 0.00108 mol/L - 0.0108 mol/L. After reaction, sample images were collected and RGB values were analyzed, as shown in Figure S1.

Optimization of pH: The pH of the sensing system was adjusted using 0.1 mol/L H_2SO_4 or NaOH solutions. The RGB values of colorimetric PAAHM sensors after absorbing 20 μL of 1×10^{-4} mol/L PO_4^{3-} solution under different pH conditions were recorded and analyzed (Figure S1).

6.2. Condition optimization of NH_4^+ colorimetric PAAHM sensor

Optimization of pH: The pH of the sensing system was adjusted using 0.1 mol/L HCl or NaOH solutions. The RGB values of the colorimetric PAAHM sensors after absorbing 10 μL of 0.0143 mol/L NH_4^+ solution at different pH values were recorded and analyzed, as summarized in Figure S1.

7. Detection the actual sample of UV-Vis spectrophotometric method

Detection of NH_4^+ concentration in water samples[3]: A defined volume of the pre-distilled water sample was taken, followed by the addition of 1 mL potassium antimony citrate solution (0.272 mol/L) with stirring. Subsequently, 1.5 mL of Nessler's reagent was added. After standing for 20 min, the absorbance was measured at 420 nm. The NH_4^+ concentration was calculated and compared with the results obtained using the hydrogel microsphere sensor.

Detection of PO_4^{3-} concentration in water samples[4]: A defined volume of the water sample was mixed with 1 mL of ascorbic acid solution (0.568 mol/L), followed by the addition of 1 mL potassium antimony tartrate (0.0108 mol/L) and 1.5 mL ammonium molybdate solution (0.0527 mol/L). The pH was adjusted to 3.0. After 20 min of reaction, the absorbance was measured at 700 nm, and the results were compared with those obtained using the microsphere sensor.

Detection of Fe^{2+} concentration in water samples[5]: A defined volume of the water sample was mixed with 5 mL of Hac-NaAc buffer solution and 2 mL of 1,10-phenanthroline solution. After a reaction time of 10 min, the absorbance was recorded at 510 nm. The Fe^{2+} concentration was calculated and compared with the microsphere sensor results.

8. Hardware and software configuration

All computational procedures were implemented using the Python programming language. Image dataset preprocessing was conducted using the Python Imaging Library (PIL), while pixel-level data extraction was performed with OpenCV. NumPy was utilized to convert the pixel information into structured numerical matrices. All experiments were conducted on a Microsoft Windows 10 (x64) operating system equipped with an Intel Core i5-5200U CPU and 12 GB of RAM. The development environment was Visual Studio Code, version 1.76.2.

Two deep learning architectures, namely Convolutional Neural Network (CNN) and Artificial Neural Network (ANN), were implemented using the PyTorch framework. Additionally, five classical machine learning algorithms were employed for comparative analysis: Extreme Gradient Boosting (XGBoost), Decision Tree (DT), K-Nearest Neighbors (KNN), Random Forest (RF), and Support Vector Machine (SVM). The XGBoost model was implemented using the official XGBoost library, whereas the remaining machine learning models were constructed using the scikit-learn library.

For data input, the CNN model was configured to process raw images directly, enabling automatic feature extraction. In contrast, the ANN and traditional machine learning models required prior segmentation of the regions of interest (ROIs) within the images. Subsequently, the RGB pixel values from these ROIs were extracted and

formatted as structured feature vectors to serve as inputs for model training and inference.

9. Data collection

9.1. Data collection for NH_4^+ colorimetric PAAHM sensors

Volumes of 5, 10, and 15 μL of NH_4^+ sample solutions were added to the colorimetric PAAHM sensors. Optical images were acquired using an SHL-500 camera and S-EYE software. The SHL-500 electronic camera was set to 1920×1080 resolution and format, MJPG format, exposure time -8, gain 0, color temperature 6200, brightness 0, contrast 6, saturation 90, gamma 119, sharpness 1, and light source frequency 50 Hz.

9.2. Data collection for PO_4^{3-} colorimetric PAAHM sensors

Volumes of 10, 20, and 30 μL of PO_4^{3-} sample solutions were added to the sensors, and corresponding optical images were recorded using an SHL-500 camera and S-EYE software. The SHL-500 electronic camera was set to 1920×1080 resolution and format, MJPG format, exposure time -8, gain 0, color temperature 5900, brightness 18, contrast 0, saturation 63, gamma 111, sharpness 2, and light source frequency 50 Hz.

9.3. Data collection for Fe^{2+} colorimetric PAAHM sensors

Volumes of 10, 20, and 30 μL of Fe^{2+} sample solutions were added to the sensors and the colorimetric response optical image was acquired using the SHL-500 electronic camera and S-EYE photography software. The SHL-500 electronic camera was set to 1920×1080 resolution and format, MJPG format, exposure time -8, gain 0, color temperature 6500, brightness 0, contrast 0, saturation 73, gamma 115, sharpness 10, and light source frequency 50 Hz.

10. Volume self-correcting method

A volume self-calibrated RGB correction model was employed to compensate for variations in sample volume:

$$\frac{B_n}{B_2} = \left(\frac{V_n}{V_2}\right)^{x_i} \quad (1)$$

$$\bar{x} = \frac{\Sigma_{i=1}^{n} x_i}{n} \quad (2)$$

$$B'_n = \frac{B_n}{\left(\frac{V_n}{V_2}\right)^{\bar{x}}} \quad (3)$$

In this model, V_2 represents the reference volume and V_n represents the other sample volumes. B_n denotes the corresponding color rendering parameter (B value). The correction factor x_i was obtained by fitting the measured B and V values using Equation (1). The average correction factor was calculated using Equation (2), and the corrected color rendering parameter B'_n was subsequently obtained using Equation (3).

11. Quantification modeling

The total number of unreplicated colorimetric images of the three ionic markers (NH_4^+, PO_4^{3-}, Fe^{2+}) of the water samples were obtained as the dataset, and 7740 photographs were accumulated, and the total dataset was divided into three subsets in the ratio of 8:1:1: the training set, the validation set, and the unlabeled training set. The architecture of the CNN quantitative model is summarized in Table S2. Each image was cropped to 760×690 pixels for input into the training, validation, and test sets. The loss function was defined as cross-entropy and stochastic optimization was performed using adaptive moment estimation (Adam). The learning rate was set to 0.0001 and the batch sizes were all 64. The structure of the ANN quantitative model is summarized in Table S3-5. The optimization and evaluation methods of this model are the same as those of the CNN quantitative model. The learning rate was set to 0.0001, and the batch sizes for both the training and validation sets were 128, with a total of 1,000 calendar elements trained.

Results and analysis

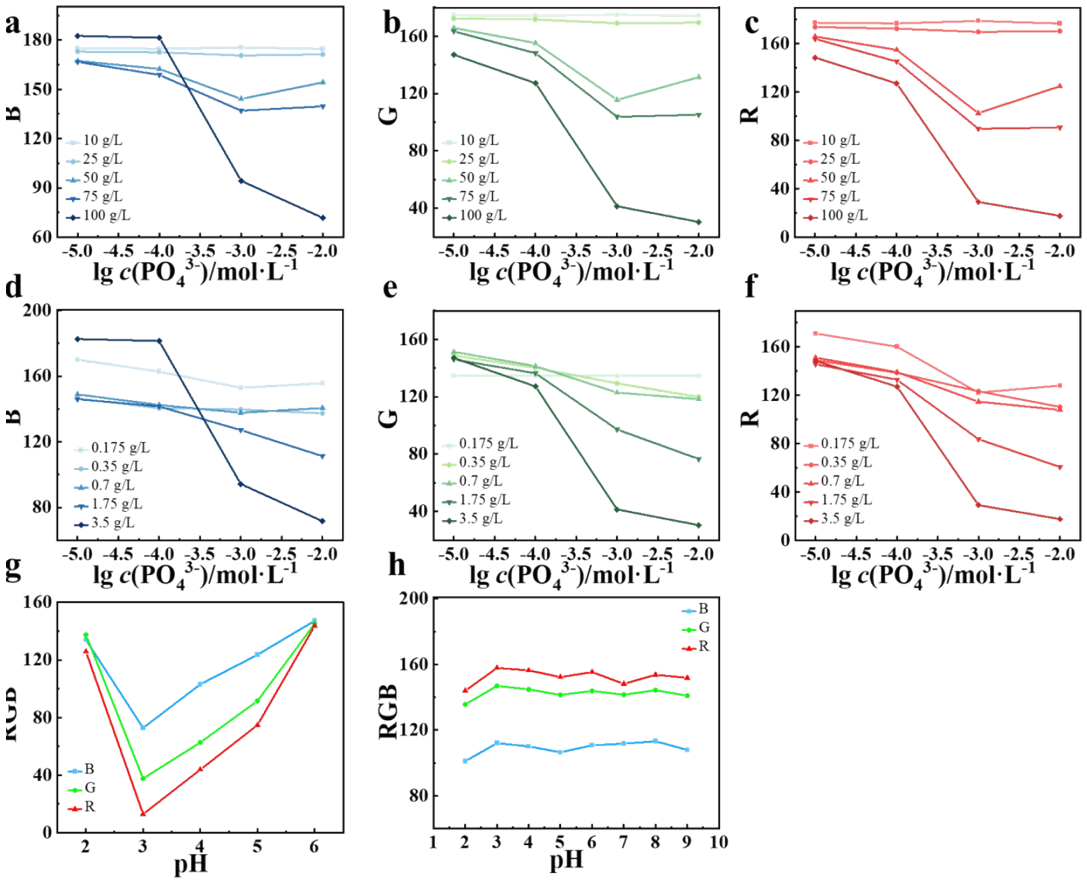

Figure S1. (a) B, (b) G and (c) R values for different concentrations of ascorbic acid (AA); (d) B, (e) G and (f) R values for different concentrations of antimony potassium tartrate. RGB values of colorimetric PAAHM sensors at different pH conditions for the detection of (g) NH_4^+ and (h) PO_4^{3-}.

Different indicator amounts resulted in distinct color development behaviors. To determine the optimal indicator concentration with the highest discrimination capability under identical concentration gradients, the effects of different concentrations of AA and potassium antimony tartrate on the RGB values of PO_4^{3-} were investigated. Comparing Fig. S1 (a-c), only the concentration of AA at 0.568 mol /L showed a consistent trend of RGB values and it also had the best discriminating ability for PO_4^{3-} at all concentrations. Observing Fig. S1 (d-f), the RGB values of potassium antimony tartrate at concentrations of 0.00540 mol/L and 0.0108 mol/L showed the same trend of variation with concentration, with the 0.0108 mol/L potassium antimony tartrate showing a greater variation. Therefore, 0.568 mol /L of AA solution and 0.0108 mol/L of antimony potassium tartrate solution were selected in the subsequent experiments.

In addition, observing the Fig. S1 (g-h), it was determined that the optimal pH for the colorimetric indicator used for the detection of PO_4^{3-} was 3.0, while the colorimetric indicator used for the detection of NH_4^+ was less affected by pH.

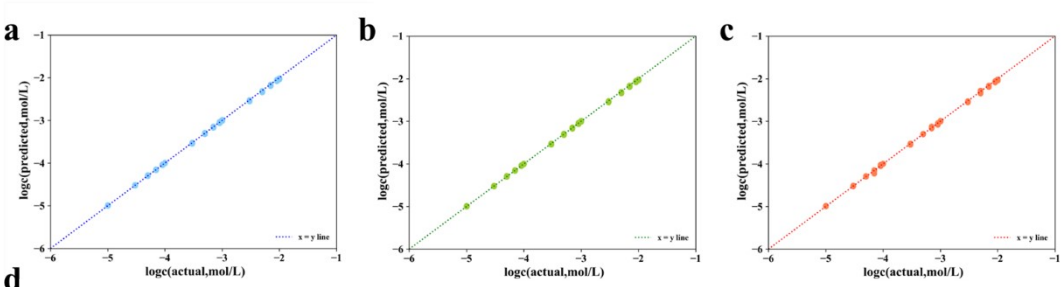

d

Evaluation Indicators	Training Set	Validation Set	Testing Set
R^2	0.999	0.999	0.999
MSE	0.000	0.000	0.001
RMSE	0.017	0.016	0.029
MAE	0.013	0.013	0.017

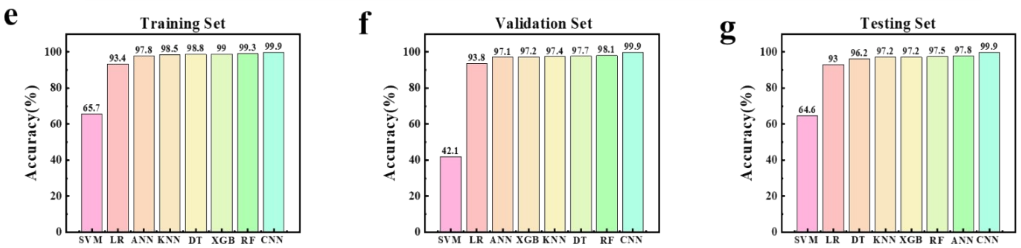

Figure S2. Performance of DL-assisted self-volume-calibrating colorimetric PAAHM sensors for Fe^{2+} quantitative detection. Actual vs predicted concentration for the (a) training set, (b) validation set and (c) test set. (d) Four evaluation indicators of quantification accuracy based on the CNN models. Comparison of prediction accuracies by employing different quantification models on the (e) training set, (f) validation set and (g) testing set.

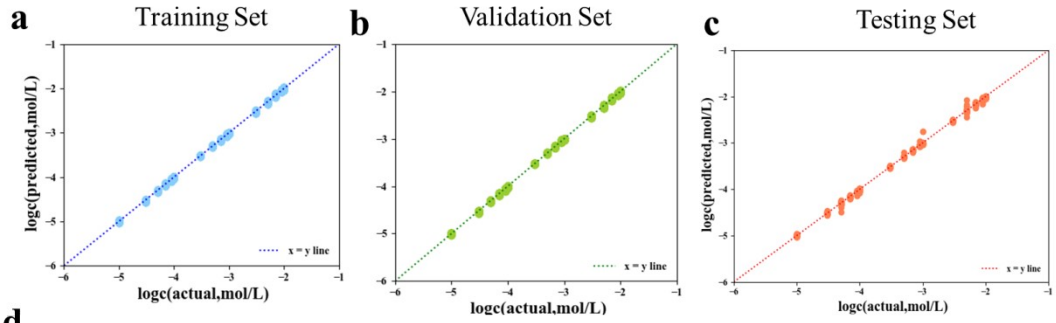

d

Evaluation Indicators	Training Set	Validation Set	Testing Set
R^2	0.999	0.999	0.999
MSE	0.000	0.000	0.001
RMSE	0.017	0.016	0.029
MAE	0.013	0.013	0.017

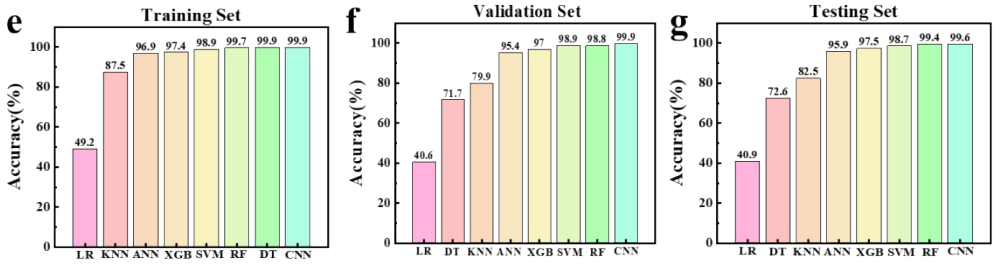

Figure S3. Performance of DL-assisted self-volume-calibrating colorimetric PAAHM sensors for PO_4^{3-} quantitative detection. Actual vs predicted concentration for the (a) training set, (b) validation set and (c) test set. (d) Four evaluation indicators of quantification accuracy based on the CNN models. Comparison of prediction accuracies by employing different quantification models on the (e) training set, (f) validation set and (g) testing set.

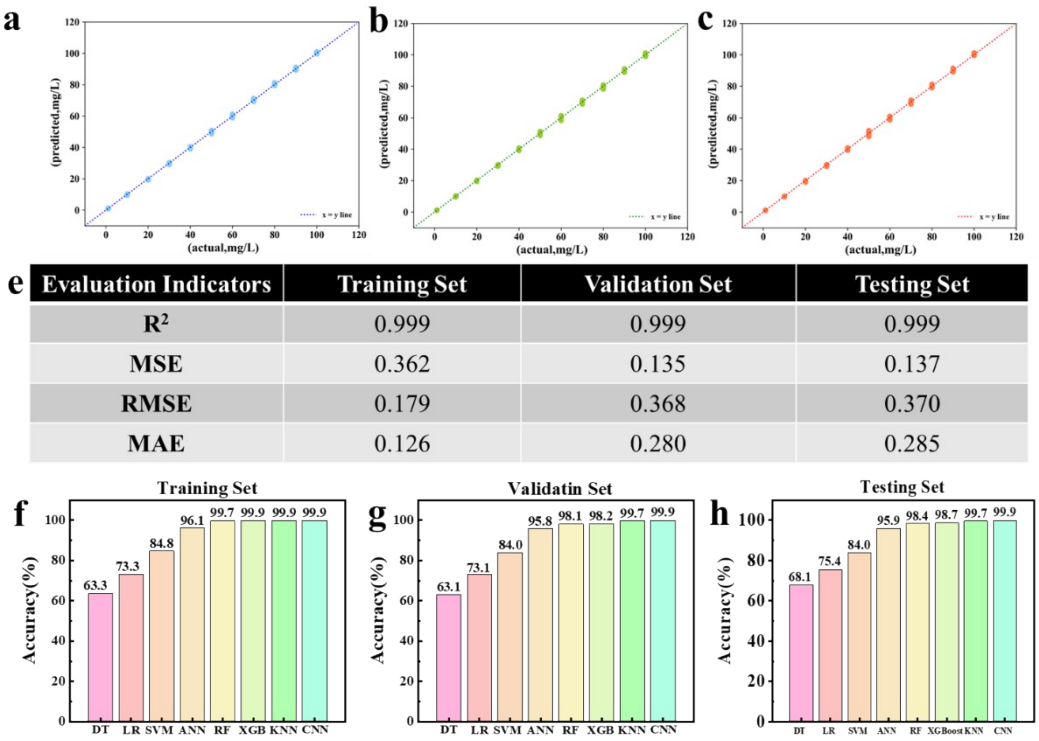

Evaluation Indicators	Training Set	Validation Set	Testing Set
R^2	0.999	0.999	0.999
MSE	0.362	0.135	0.137
RMSE	0.179	0.368	0.370
MAE	0.126	0.280	0.285

Figure S4. Performance of DL-assisted self-volume-calibrating colorimetric PAAHM sensors for NH_4^+ quantitative detection. Actual vs predicted concentration for the (a) training set, (b) validation set and (c) test set. (d) Four evaluation indicators of quantification accuracy based on the CNN models. Comparison of prediction accuracies by employing different quantification models on the (e) training set, (f) validation set and (g) testing set.

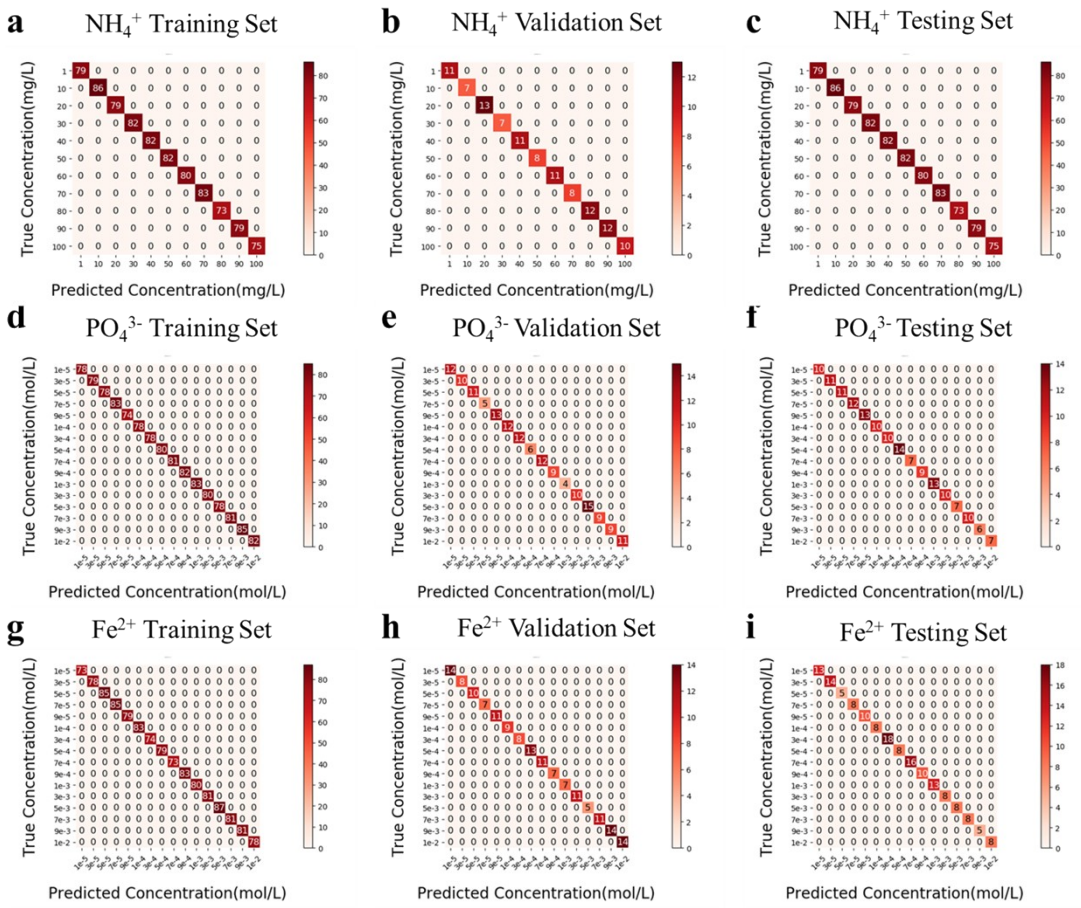

Figure S5. CNN model for the classification of (a-c) 1.87-10 mg/L NH_4^+, (d-f) 1×10^{-5}-1×10^{-2} mol/L PO_4^{3-}, (g-i) 1×10^{-5}-1×10^{-2} mol/L Fe^{2+}.

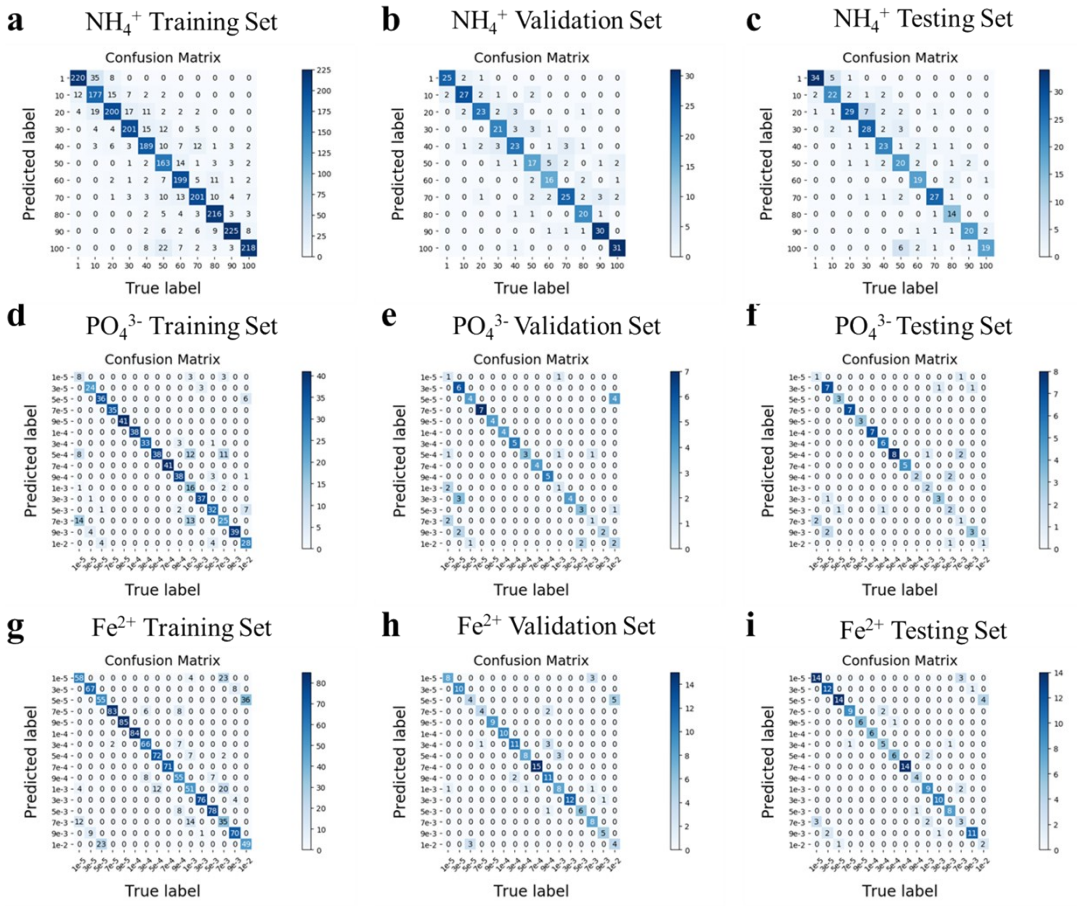

Figure S6. ANN model for the classification of (a-c) 1-10 mg/L NH_4^+, (d-f) 1×10^{-5}-1×10^{-2} mol/L PO_4^{3-}, (g-i) 1×10^{-5}-1×10^{-2} mol/L Fe^{2+}.

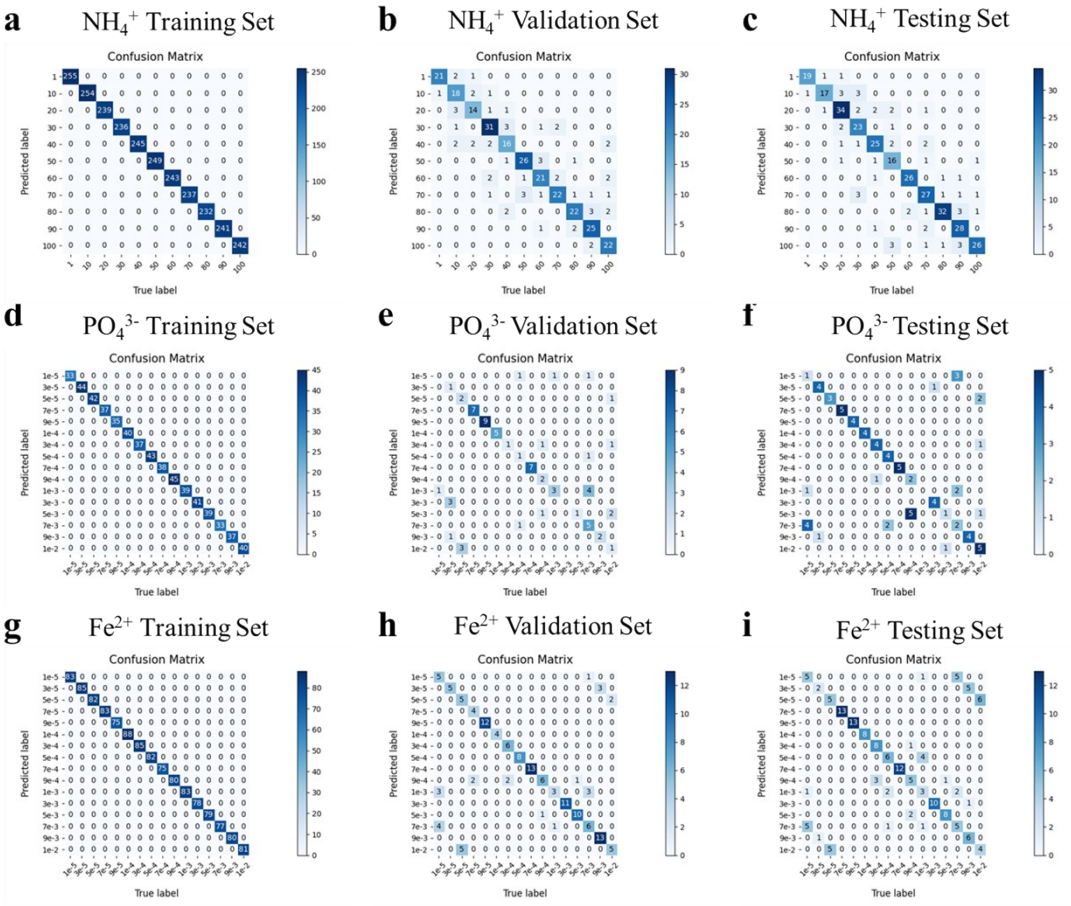

Figure S7. DT model for the classification of (a-c) 1-10 mg/L NH_4^+, (d-f) 1×10^{-5}-1×10^{-2} mol/L PO_4^{3-}, (g-i) 1×10^{-5}-1×10^{-2} mol/L Fe^{2+}.

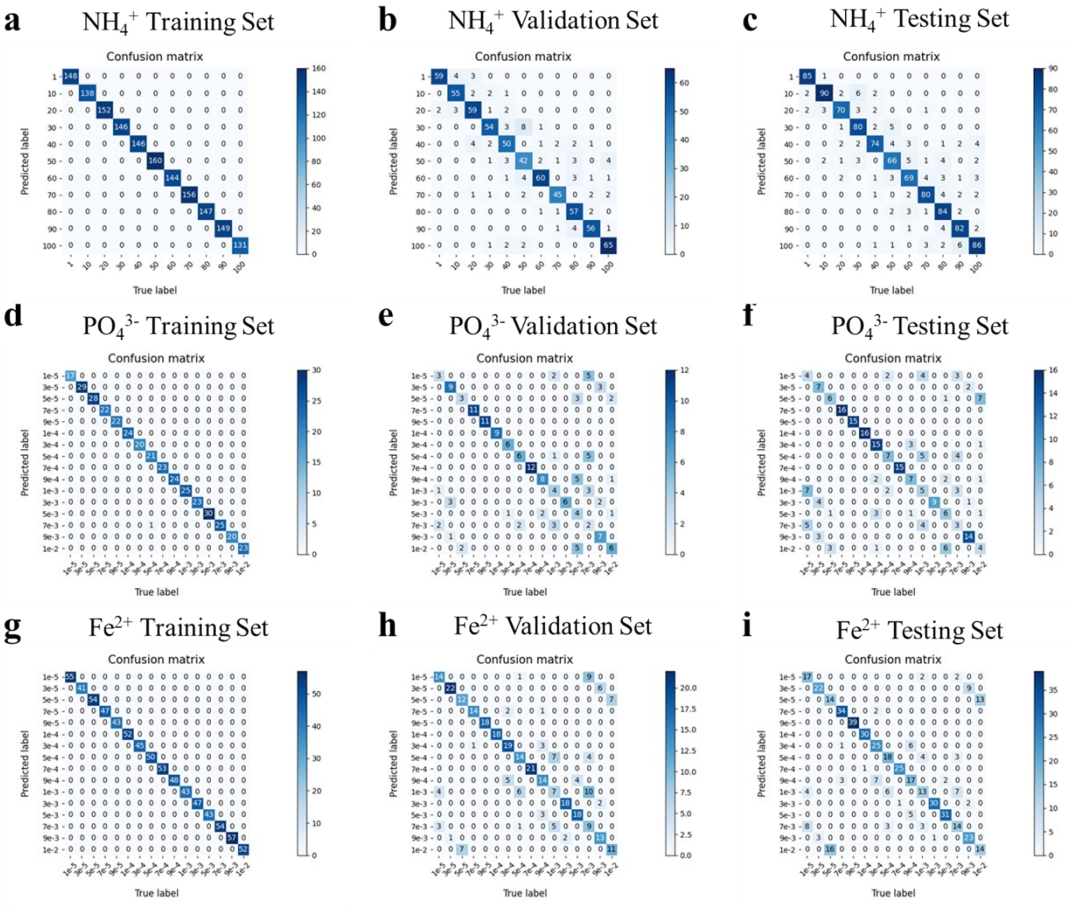

Figure S8. KNN model for the classification of (a-c) 1-10 mg/L NH_4^+, (d-f) 1×10^{-5}-1×10^{-2} mol/L PO_4^{3-}, (g-i) 1×10^{-5}-1×10^{-2} mol/L Fe^{2+}.

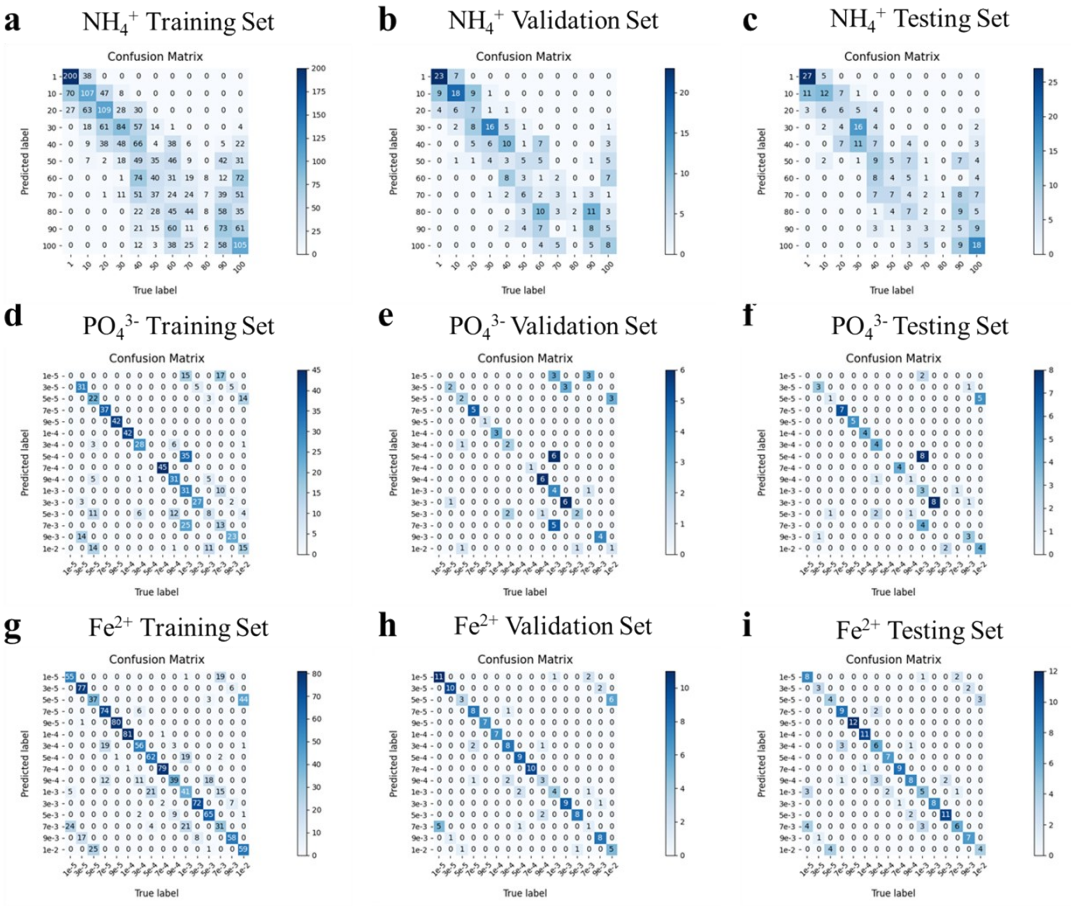

Figure S9. LR model for the classification of (a-c) 1-10 mg/L NH_4^+, (d-f) 1×10^{-5}-1×10^{-2} mol/L PO_4^{3-}, (g-i) 1×10^{-5}-1×10^{-2} mol/L Fe^{2+}.

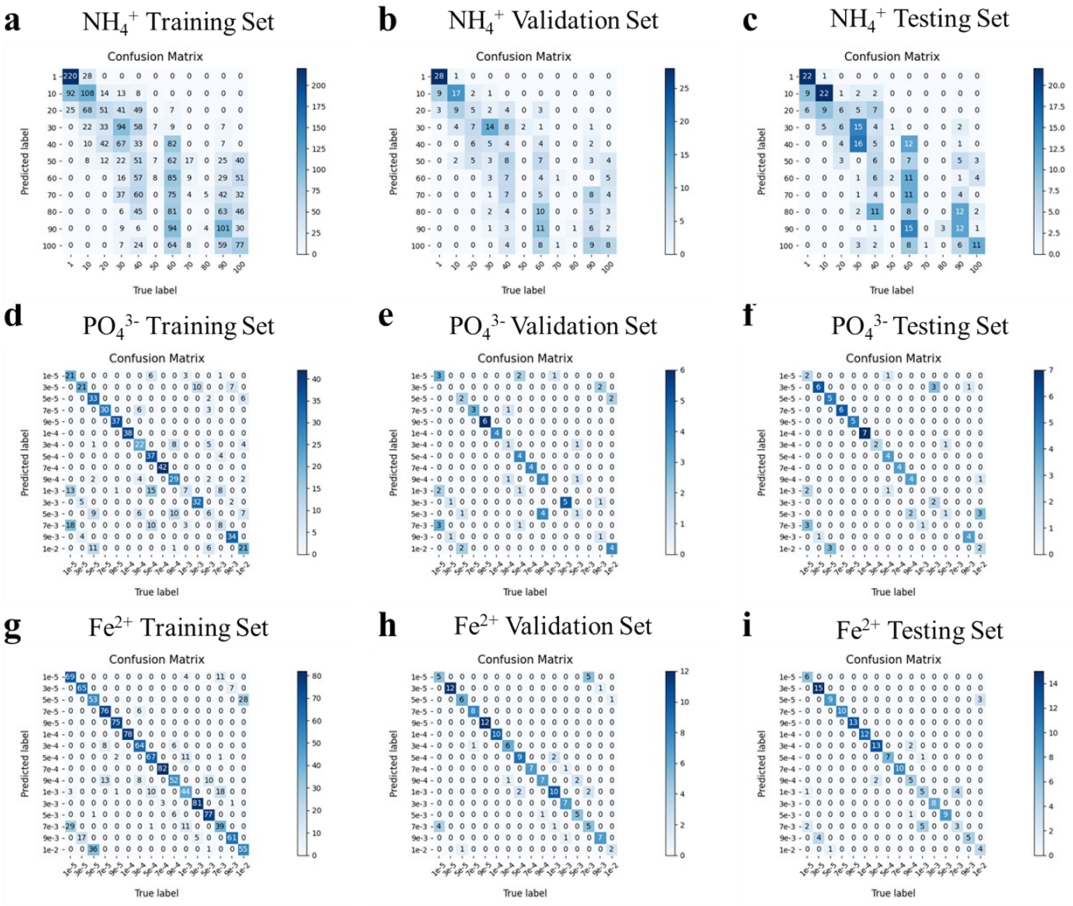

Figure S10. NB model for the classification of (a-c) 1-10 mg/L NH_4^+, (d-f) 1×10^{-5}-1×10^{-2} mol/L PO_4^{3-}, (g-i) 1×10^{-5}-1×10^{-2} mol/L Fe^{2+}.

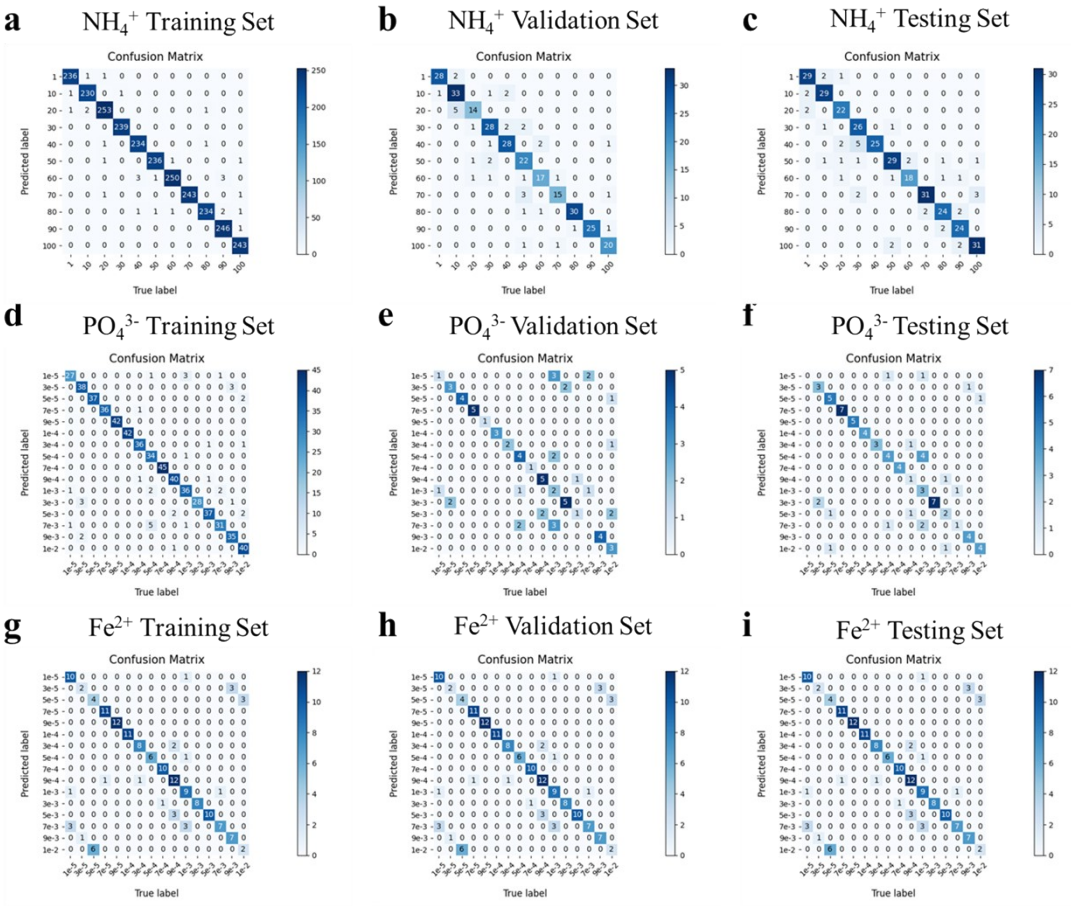

Figure S11. RF model for the classification of (a-c) 1-10 mg/L NH_4^+, (d-f) 1×10^{-5}-1×10^{-2} mol/L PO_4^{3-}, (g-i) 1×10^{-5}-1×10^{-2} mol/L Fe^{2+}.

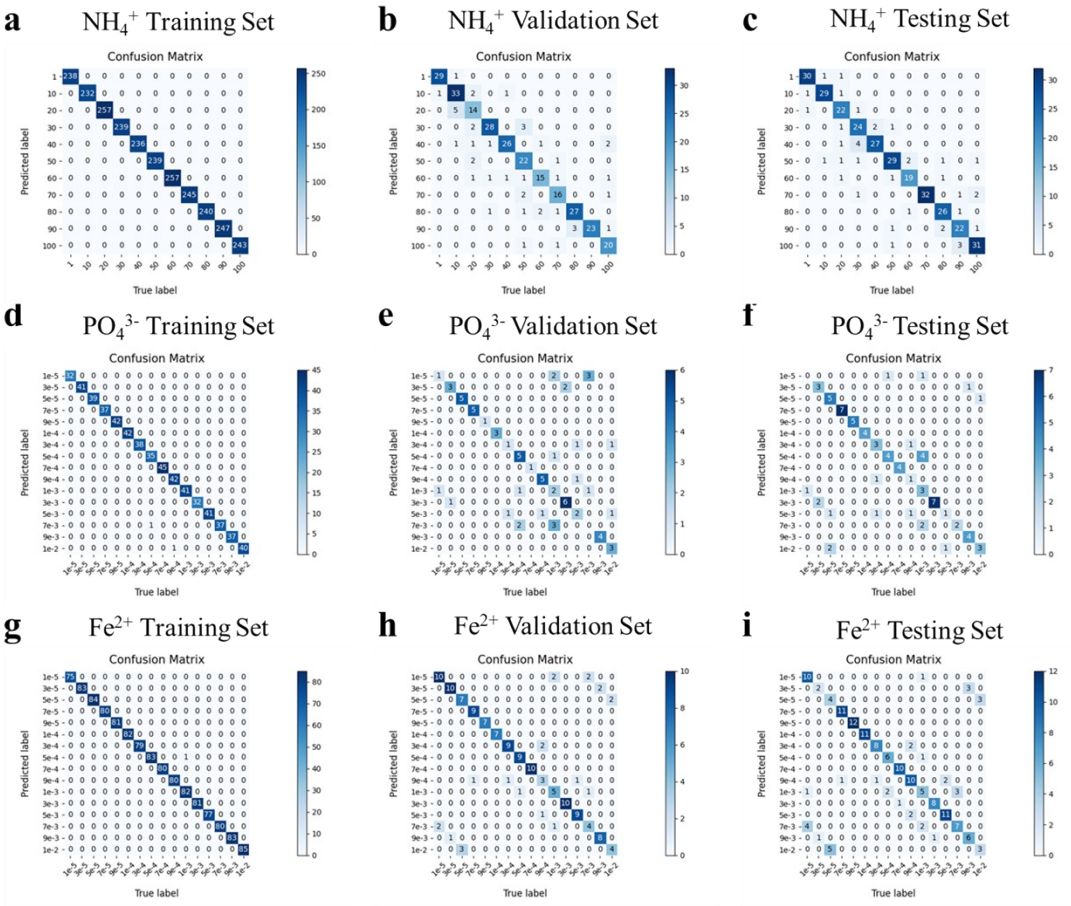

Figure S12. XGB model for the classification of (a-c) 1-10 mg/L NH_4^+, (d-f) 1×10^{-5}-1×10^{-2} mol/L PO_4^{3-}, (g-i) 1×10^{-5}-1×10^{-2} mol/L Fe^{2+}.

Figure S13. SVM model for the classification of (a-c) 1-10 mg/L NH_4^+, (d-f) 1×10^{-5}-1×10^{-2} mol/L PO_4^{3-}, (g-i) 1×10^{-5}-1×10^{-2} mol/L Fe^{2+}.

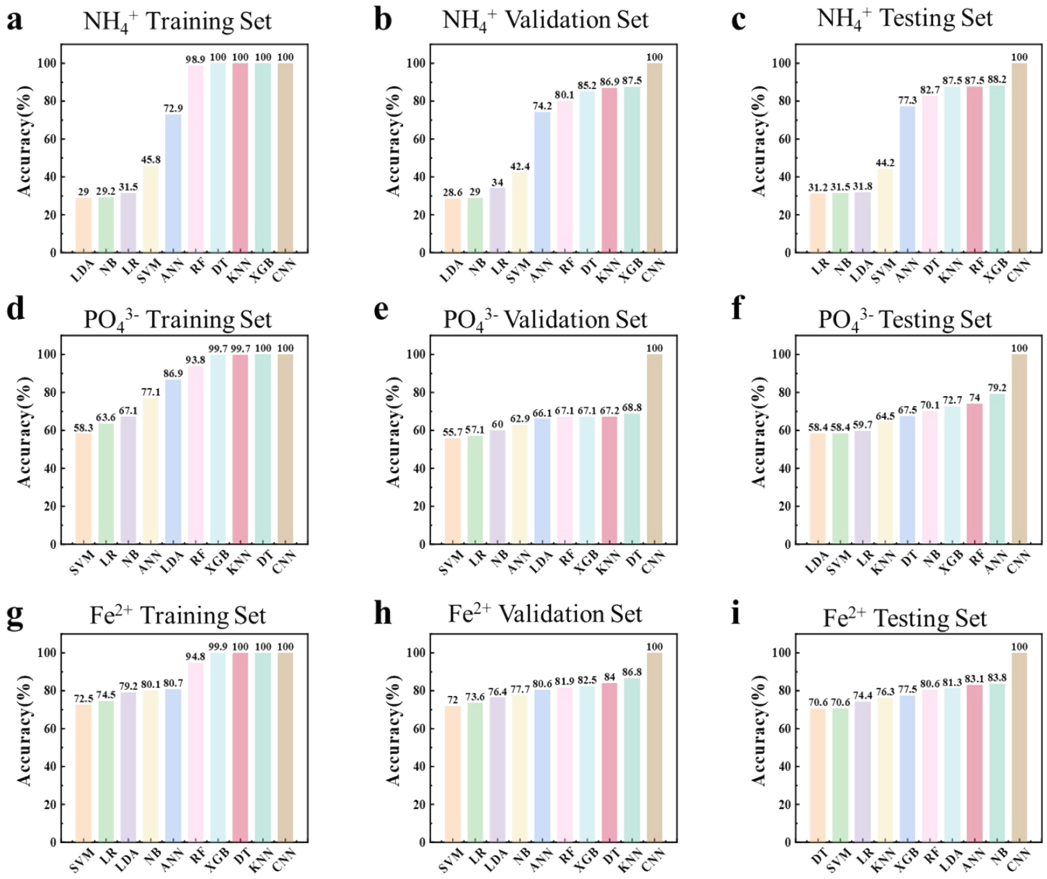

Figure S14. Comparison of classify accuracies by employing different classification models on the (a-c) 1-10 mg/L NH_4^+, (d-f) 1×10^{-5}-1×10^{-2} mol/L PO_4^{3-}, (g-i) 1×10^{-5}-1×10^{-2} mol/L Fe^{2+}.

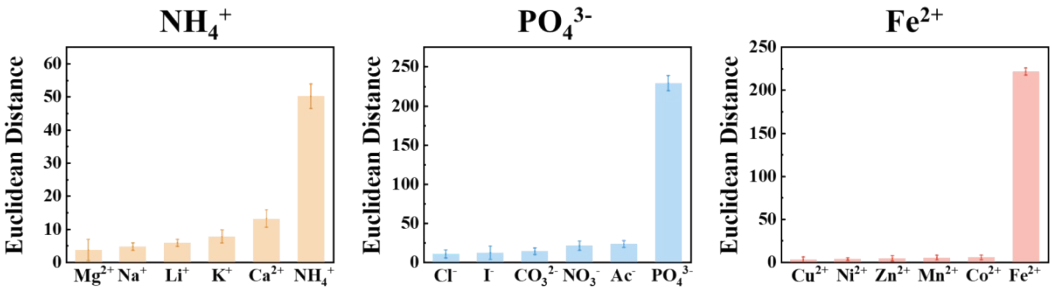

Figure S15. Selectivity of (a) NH_4^+, (b) PO_4^{3-}, and (c) Fe^{2+}in PAAHM sensor.

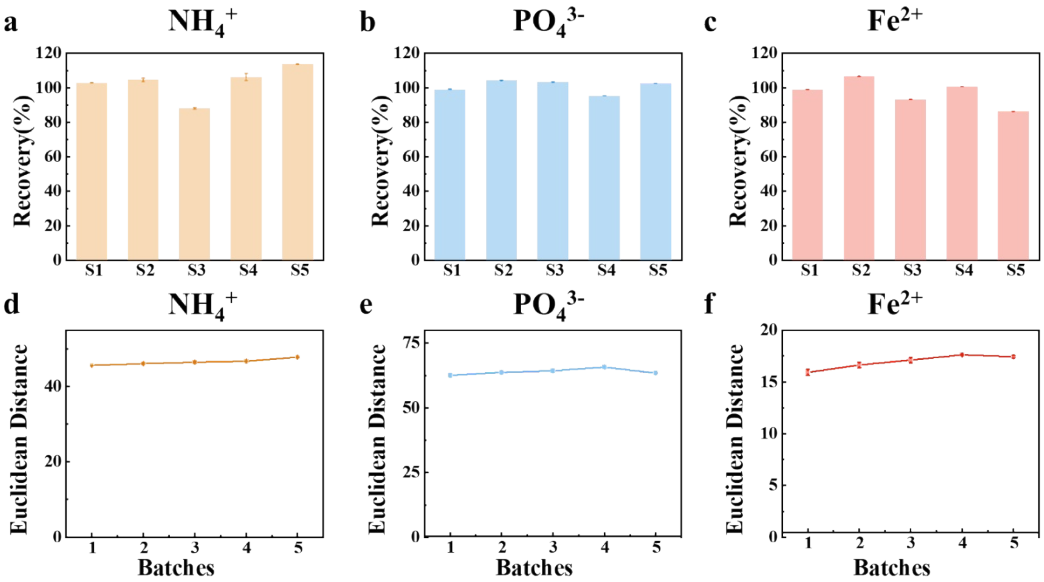

Figure S16. Spiked recovery rate of (a) NH_4^+, (b) PO_4^{3-}, and (c) Fe^{2+}. Euclidean distance of different batches PAAHM (d) NH_4^+ (7.48×10^{-4} mol/L), (e) PO_4^{3-} (1×10^{-5} mol/L), and (f) Fe^{2+} (1×10^{-5} mol/L) in PAAHM sensor.

Table S1. Actual water samples

NO.	Type	Source
1	Surface water	Guangzhou Airport Sewage Treatment Plant Inlet (located at 23.3925° north latitude and 113.2988° east longitude of Guangzhou City, Guangdong Province).
2		Hai Tao Phase III Inlet (located at 23.0360° north latitude and 113.4965° east longitude of Guangzhou City, Guangdong Province).
3		Qian Feng Phase I & II Inlet (located at 23.0844° north latitude and 113.3168° east longitude of Guangzhou City, Guangdong Province).
4		Li Jiao Phase I & II Inlet (located at 23.0600° north latitude and 113.3190° east longitude of Guangzhou City, Guangdong Province).
5		Lie De Phase I & II Inlet (located at 23.1130° north latitude and 113.3390° east longitude of Guangzhou City, Guangdong Province).

Table S2. The architecture of the CNN quantification model

Layer	Layer (type)	Output Shape
1	Input layer	(None, 100, 100, 3)
2	Convolution layer	(None, 98, 98, 32)
3	Max pooling layer	(None, 49, 49, 32)
4	Convolution layer	(None, 47, 47, 64)
5	Max pooling layer	(None, 23, 23, 64)
6	Convolution layer	(None, 21, 21, 128)
7	Max pooling layer	(None, 10, 10, 128)
8	Convolution layer	(None, 8, 8, 128)
9	Max pooling layer	(None, 4, 4, 128)
10	Flatten layer	(None, 2048)
11	Fully-connected layer	(None, 128)
12	Dropout layer	(None, 128)
13	Fully-connected layer	(None, 1)
14	Output	(None, 1)

Table S3. The architecture of the ANN quantification model for PO_4^{3-}.

Layer	Layer (type)	Output Shape
1	Input layer	(None, 3)
2	Fully-connected layer	(None, 256)
3	Fully-connected layer	(None, 1024)
4	Fully-connected layer	(None, 512)
5	Dropout layer	(None, 256)
6	Fully-connected layer	(None, 1)
7	Output	(None, 1)

Table S4. The architecture of the ANN quantification model for NH_4^+.

Layer	Layer (type)	Output Shape
1	Input layer	(None, 3)
2	Fully-connected layer	(None, 64)
3	Fully-connected layer	(None, 256)
4	Fully-connected layer	(None, 128)
5	Dropout layer	(None, 64)
6	Fully-connected layer	(None, 1)
7	Output	(None, 1)

Table S5. The architecture of the ANN quantification model for Fe^{2+}.

Layer	Layer (type)	Output Shape
1	Input layer	(None, 3)
2	Fully-connected layer	(None, 128)
3	Fully-connected layer	(None, 256)
4	Fully-connected layer	(None, 1024)
5	Dropout layer	(None, 512)
6	Fully-connected layer	(None, 1)
7	Output	(None, 1)

Table S6. Parameters of ML quantification models for NH_4^+.

Algorithm	Parameters
XGB	(num_round = 360, eta = 0.05, max_dept = 6, subsample = 0.75)
Decision Trees	(criterion = ' mae', splitter = ' best', max_depth = 21, min_samples_leaf = 1, min_samples_split = 2)
KNN	(n_neighbors = 3, weights = 'uniform', algorithm = 'auto', leaf_size = 30, p = 2, metric = 'minkowski')
Random Forest	(criterion = ' mae ', n_estimators = 41, max_depth = 17, min_samples_leaf = 1, min_samples_split = 2)
SVM	(kernel = 'rbf', gamma = 1.68, C = 2.46)

Table S7. Parameters of ML quantification models for PO_4^{3-}.

Algorithm	Parameters
XGB	(num_round = 100, eta = 0.1, max_dept = 7, subsample = 0.55)
Decision Trees	(criterion = ' absolute_error', splitter = ' best', max_depth = 35, min_samples_leaf = 1, min_samples_split = 2)
KNN	(n_neighbors = 5, weights = 'uniform', algorithm = 'auto', leaf_size = 30, p = 2, metric = 'minkowski')
Random Forest	(criterion = ' squared_error ', n_estimators = 1, max_depth = 5, min_samples_leaf = 1, min_samples_split = 2)
SVM	(kernel = 'rbf', gamma = 3.16, C = 1000)

Table S8. Parameters of ML quantification models for Fe^{2+}

Algorithm	Parameters
XGB	(num_round = 100, eta = 0.3, max_dept = 7, subsample = 0.9)
Decision Trees	(criterion = 'mae', splitter = 'random', max_depth = 27, min_samples_leaf = 2, min_samples_split = 2)
KNN	(n_neighbors = 3, weights = 'uniform', algorithm = 'auto', leaf_size = 30, p = 2, metric = 'minkowski')
Random Forest	(criterion = ' mae ', n_estimators = 41, max_depth = 28, min_samples_leaf = 1, min_samples_split = 8)
SVM	(kernel = 'rbf', gamma = 1, C = 1000)

Table S9. Quantification performance for PO_4^{3-} on the three sub-datasets based on different quantification models.

□	**Training set**							
	XGB	**DT**	**KNN**	**LR**	**RF**	**SVM**	**ANN**	**CNN**
R^2	0.975	0.999	0.875	0.492	0.997	0.990	0.970	0.999
MSE	84.589	4.295	1.346	5.654	8.890	34.773	0.025	0.001
RMSE	9.197	6.554	0.001	0.002	2.983	5.897	0.159	0.016
MAE	7.105	2.520	0.001	0.001	0.843	3.478	0.102	0.013
□	**Validation set**							
	XGB	**DT**	**KNN**	**LR**	**RF**	**SVM**	**ANN**	**CNN**
R^2	0.970	0.717	0.798	0.407	0.988	0.990	0.955	0.999
MSE	93.834	3.019	2.462	6.486	36.905	30.591	0.038	0.001
RMSE	9.687	0.002	0.001	0.003	6.075	5.531	0.195	0.016
MAE	7.510	0.001	0.001	0.002	2.480	3.432	0.119	0.012
□	**Testing set**							
	XGB	**DT**	**KNN**	**LR**	**RF**	**SVM**	**ANN**	**CNN**
R^2	0.976	0.726	0.825	0.409	0.994	0.988	0.959	0.999
MSE	80.218	2.930	2.077	5.864	18.827	40.113	0.036	0.001
RMSE	8.956	0.002	0.001	0.002	4.339	6.333	0.190	0.029
MAE	6.897	0.001	0.001	0.002	2.034	3.623	0.113	0.017

Table S10. Quantification performance for NH_4^+ on the three sub-datasets based on different quantification models.

□	**Training set**							
	XGB	**DT**	**KNN**	**LR**	**RF**	**SVM**	**ANN**	**CNN**
R^2	0.983	0.983	0.972	0.687	0.987	0.782	0.914	0.999
MSE	17.074	16.630	27.592	313.049	12.126	218.984	85.436	0.362
RMSE	4.132	4.078	5.253	17.693	3.482	14.798	9.243	0.179
MAE	2.909	0.725	1.837	14.448	1.961	11.018	6.525	0.126
□	**Validation set**							
	XGB	**DT**	**KNN**	**LR**	**RF**	**SVM**	**ANN**	**CNN**
R^2	0.910	0.796	0.920	0.679	0.928	0.776	0.881	0.999
MSE	82.553	187.505	82.386	294.381	66.324	205.705	123.063	0.135
RMSE	9.086	13.693	9.077	17.158	8.144	14.342	11.093	0.368
MAE	6.128	5.828	3.984	14.0149	4.867	10.629	7.821	0.280
□	**Testing set**							
	XGB	**DT**	**KNN**	**LR**	**RF**	**SVM**	**ANN**	**CNN**
R^2	0.934	0.881	0.932	0.706	0.946	0.813	0.882	0.999
MSE	64.243	116.269	67.981	286.979	53.181	182.882	108.777	0.137
RMSE	8.015	10.783	8.245	16.940	7.293	13.523	10.423	0.370
MAE	5.358	4.336	3.340	13.612	4.218	10.098	7.343	0.285

Table S11. Quantification performance for Fe^{2+} on the three sub-datasets based on different quantification models.

□	**Training set**							
	XGB	**DT**	**KNN**	**LR**	**RF**	**SVM**	**ANN**	**CNN**
R^2	0.990	0.988	0.985	0.934	0.993	0.657	0.972	0.999
MSE ($\times 10^{-7}$)	1.08	1.24	1.54	7.18	7.25	1.81	3.00	0.001
RMSE	0.001	0.001	0.001	0.001	0.000	0.004	0.001	0.015
MAE	0.001	8.87e-5	0.001	0.001	9.205 e-5	0.004	0.000	0.001
□	**Validation set**							
	XGB	**DT**	**KNN**	**LR**	**RF**	**SVM**	**ANN**	**CNN**
R^2	0.972	0.977	0.974	0.938	0.981	0.421	0.971	0.999
MSE ($\times 10^{-7}$)	3.40	2.84	2.57	7.65	2.32	176	3.26	0.001
RMSE	0.001	0.001	0.001	0.001	0.000	0.004	0.001	0.015
MAE	0.001	0.001	0.001	0.001	0.000	0.004	0.000	0.011
□	**Testing set**							
	XGB	**DT**	**KNN**	**LR**	**RF**	**SVM**	**ANN**	**CNN**
R^2	0.972	0.962	0.972	0.930	0.975	0.646	0.978	0.999
MSE ($\times 10^{-7}$)	2.98	4.11	3.58	7.59	2.70	179	2.8	0.001
RMSE	0.001	0.001	0.001	0.001	0.000	0.004	0.001	0.017
MAE	0.001	0.001	0.001	0.001	0.000	0.004	0.000	0.012

Table S12. Classification accuracy for NH_4^+, PO_4^{3-}, Fe^{2+} based on different classification models.

	Training set Accuracy (%)									
	XGB	**DT**	**KNN**	**LR**	**RF**	**SVM**	**LDA**	**NB**	**ANN**	**CNN**
NH_4^+	100.0	100	100	31.5	98.9	45.8	29.0	29.2	72.9	100
PO_4^{3-}	99.7	100	99.7	63.6	93.7	58.3	68.9	67.1	77.1	100
Fe^{2+}	99.9	100	100	74.5	94.8	72.5	79.2	80.1	80.7	100
	Validation set Accuracy (%)									
	XGB	**DT**	**KNN**	**LR**	**RF**	**SVM**	**LDA**	**NB**	**ANN**	**CNN**
NH_4^+	85.2	80.1	86.9	34.0	87.5	42.4	28.6	29.0	74.2	100
PO_4^{3-}	67.1	67.1	66.1	55.7	62.9	57.1	67.1	60.0	68.8	100
Fe^{2+}	84.0	80.6	72.0	76.4	86.8	73.6	77.8	81.9	82.5	100
	Testing set Accuracy (%)									
	XGB	**DT**	**KNN**	**LR**	**RF**	**SVM**	**LDA**	**NB**	**ANN**	**CNN**
NH_4^+	88.2	82.7	87.5	31.2	87.5	44.2	31.8	31.5	77.3	100
PO_4^{3-}	72.7	67.5	64.5	59.7	74.0	58.4	58.4	70.1	79.2	100
Fe^{2+}	77.5	70.6	76.3	74.4	80.6	70.6	81.3	83.8	83.1	100

Table S13. Relative Standard Deviation，Relative Bias and Relative Expanded Uncertainty of NH_4^+, PO_4^{3-}, and Fe^{2+} PAAHM sensor.

	NH_4^+			PO_4^{3-}			Fe^{2+}		
	Relative Standard Deviation/%	**Relative Bias%**	**Relative Expanded Uncertainty/%**	**Relative Standard Deviation/%**	**Relative Bias%**	**Relative Expanded Uncertainty/%**	**Relative Standard Deviation/%**	**Relative Bias%**	**Relative Expanded Uncertainty/%**
S1	1.21	-0.33	1.41	3.14	-2.85	3.73	0.67	4.17	0.77
S2	0.41	-1.73	0.47	1.53	-4.33	1.76	2.14	-1.36	2.53
S3	1.72	-1.73	1.95	0.77	-3.03	0.89	2.59	-4.41	3.05
S4	0.85	0.21	0.97	0.74	-6.18	0.86	1.89	2.81	2.23
S5	0.76	2.24	0.87	0.68	3.41	0.79	0.20	-0.17	0.23

References

1. ISO 5667-3:2024, *Water quality - Sampling - Part 3: Preservation and handling of water samples*; International Organization for Standardization: Geneva, Switzerland, 2024
2. HJ 535-2009, *Water quality - Determination of ammonia nitrogen - Distillation-spectrophotometric method*; Ministry of Environmental Protection of China: Beijing, China, 2009.
3. W. Xiong, Z. Guo, S. Zhao, Q. Wang, Q. Xu and X. Wang, *J. Mater. Chem. A*, 2019, **7**, 19977-19983.
4. N. K. Ibnul and C. P. Tripp, *Talanta*, 2022, **238**, 123043.
5. H. Tamura, K. Goto, T. Yotsuyanagi and M. Nagayama, *Talanta*, 1974, **21**, 314-318.